Virginia Commonwealth University
VCU Scholars Compass

Theses and Dissertations

Graduate School

2014

Modeling Acute Changes in Bladder Wall Tension, Shape and Compliance During Filling

Firdaweke Habteyes
Virginia Commonwealth University

Follow this and additional works at: http://scholarscompass.vcu.edu/etd

Part of the Biomechanical Engineering Commons

Downloaded from

http://scholarscompass.vcu.edu/etd/3537

MODELING ACUTE CHANGES IN BLADDER WALL TENSION, SHAPE AND COMPLIANCE DURING FILLING

A thesis submitted in partial fulfillment of the requirements for the degree of
Master of Science at Virginia Commonwealth University

by

FIRDAWEKE GORAW HABTEYES

Director: John E. Speich, Ph.D.

Associate Professor and Associate Chair, Department of Mechanical and Nuclear Engineering

Virginia Commonwealth University, Richmond, VA, 23284

August 2014.

Dedication/Epigraph

To my mother, Bizuwork Nessibu, and my father, Goraw Habteyes who supported me all the time.

እግዚአብሔር እረኛዬ ነው ፤ የሚያሳጣኝ የለም::

መ.ዳዊት ጽ፫:፩

Say: The Lord is my shepherd, I lack nothing.

The Holy Bible, Psalm 23:1

The time to begin writing an article is when you have finished it to your satisfaction. By the time you begin clearly logically perceive what it is that you really want to say.

—Mark Twain, *Notebook*, 1902—1903

Acknowledgement

I would like to thank few people who contribute important ideas, technical guidance, faith and support to this research work. Firstly, my special gratitude goes to my advisor Dr. John Speich. I thank him for his excellent continuous follow-up, caring, patience, important comments to the project and some personal advices and experience sharing skills providing me with excellent working environment. Generally, I learn a lesson of life from Dr. Speich.

I would like to give my appreciations and thanks to Dr. James McLeskey not only serving as my thesis committee but also for his encouragement and support to my research work and for a nice conversations we used to have about everything. I would like to extend my thanks to Dr. Paul Ratz for serving as a committee and for his important comments about the project.

My unique thanks go to the Mechanical and Nuclear Engineering Director of Graduate Studies, Dr. Karla Mossi, for her assistance in my academic movements and future career. I would like to extend my thanks to Dr. Gary Tepper for his support and best suggestions. My stay in Virginia Commonwealth University would have not been possible without their kindness and help.

I would like to extend my kind thanks to my family. Foremost, my father Goraw Habteyes, my mother Bizuwork Nessibu, my oldest brothers, Tesfaye Habteyes, Habtamu Habteyes, Ashenafi Habteyes and Befekadu Habteyes, my youngest brothers Million Habteyes and Samuel Habteyes, my oldest sisters Serawit Habteyes and Tigest Habteyes and my girlfriend, Tsigemariam Demiss. They were always encouraging me and always there for me during my stay in the U.S.

Last but not least. I would like to extend my thanks to my friends, classmates and my laboratory partner, Omid Komari for their support and encouragement.

Table of Contents

List of Abbreviations

ADP…………………………………………………………………….Adenosine diphosphate

ATP…………………………………………………………………….Adenosine triphosphate

CMG…………………………………………………………………………...Cystometrogram

DSM……………………………………………………………….......Detrusor smooth muscle

HCC………………………………………………………………….Higher compliance curve

LCC………………………………………………………………...Lower compliance curve

OAB…………………………………………………………….......Overactive bladder

PBOO……………………………………………………….........Partial bladder outlet obstructed

RBC………………………………………………………………...Regulated bladder compliance

SUU…………………………………………………………………...Stand up urgency

List of Figures

Abstract

MODELING ACUTE CHANGES IN BLADDER WALL TENSION, SHAPE AND COMPLIANCE DURING FILLING

by FIRDAWEKE GORAW HABTEYES

A thesis submitted in partial fulfillment of the requirements for the degree of Master of Science at Virginia Commonwealth University.

Virginia Commonwealth University, Richmond, Virginia, 2014

Director: John E. Speich, Ph.D

Associate Professor and Associate Chair, Department of Mechanical and Nuclear Engineering

The bladder wall consists primarily of detrusor smooth muscle. Tension-sensitive nerves in the bladder wall are responsible for providing bladder fullness information that is interpreted as urgency. Bladder wall tension, and therefore nerve output, is a function of bladder volume, shape and material properties. Studies have shown that the bladder wall exhibits acutely regulated detrusor compliance. In addition, bladder shape throughout filling depends on intra-abdominal forces and material properties of the bladder wall, such as regulated detrusor compliance. This thesis focused on modeling the potential influence of acute changes in bladder compliance, shape and bladder wall tension during filling. Laplace's Law was used to demonstrate how wall tension can vary significantly with geometry in a vessel with uniform internal pressure and constant volume. A finite deformation model of the bladder was previously used to show that wall tension can increase significantly during filling with relatively little pressure change. In this thesis, published experimental data were used to determine ranges for regulated detrusor compliance, and the finite deformation model was expanded to illustrate the potential effects of regulated

detrusor compliance on filling pressure and wall tension. Also, a geometric model was used to demonstrate that constraining a perfectly spherical bladder to fill as an oblate sphere increases wall tension, and therefore should increase nerve output, for a given volume. In addition, a spheroidal model consisting of three orthogonal circular rings was developed to predict the increase in pressure and wall tension associated with deforming a spherical bladder into an oblate spheroid. Together, these models demonstrate that defects in regulated detrusor compliance and/or acute or chronic changes in bladder shape due to changes in compliance or intra-abdominal forces could contribute to changes in wall tension for a given volume that could lead to urgency.

Chapter One: Introduction and background

1.1. Motivation

Overactive bladder (**OAB**) is a symptom syndrome identified as elevated urinary **urgency** usually with increased daytime voiding frequency and nocturia (waking to voiding) in the absence of identifiable causes (Abrams & Wein, 2000). The prevalence of OAB in the US adult population is estimated at nearly 20% (Hashim & Abrams, 2007). OAB can result from bladder muscles that do not relax correctly during filling, and increased spontaneous muscle activity can cause an increased urgency (Abrams et al., 2002). OAB has a significant impact on the quality of life, such as restrictions or difficulties when it comes to travel and physical or athletic activities. Studies indicate that people with OAB have to void their urine more than eight times in a 24 hours period, and often have an urgent need to urinate that may cause them to rush to the toilet (Abrams et al., 2002). Due to the seriousness of this problem, it is important to investigate the root causes of OAB.

Clinical urodynamic studies are currently used to diagnose OAB by measuring pressure during bladder filling (Ockrim et al., 2005). There is a generally a small change in pressure during bladder filling (Frenkl et al., 2011; Watanabe, Akiyama, Saito, & Oki, 1981), however the change in wall tension is expected to be significant. Tension-sensitive nerves in the bladder wall are responsible for providing bladder fullness information that is interpreted as urgency (Kanai & Andersson, 2013). Therefore, wall tension during filling may give better information regarding urgency than pressure. Bladder wall tension, and therefore nerve output, is a function of bladder volume, shape and material properties. The overall objective of this study is to model bladder wall tension and stress during filling. This may provide valuable information for the study and diagnosis of OAB, including improved diagnostic methods or drugs used to treat OAB which target bladder smooth muscle.

The following sections give important background information about the function of the urinary bladder, bladder wall tension and pressure, smooth muscle structure and mechanics, regulated bladder compliance and bladder shape. The chapter concludes with a presentation of the thesis objectives.

1.2. Function of the bladder

The human urinary bladder is a hollow, distensible (or elastic), muscular organ positioned near the pelvic floor. The main function of the bladder is to collect urine excreted by the kidneys before disposal by urination. Urine enters the bladder by way of the ureters and exits through the urethra. Anatomically, the bladder is divided into three parts: the apex, the body and the fundus. The fundus consists of the trigone and the neck (Fig. 1.1) and is imbedded in the musculofibrous tissue in females and in the prostate in males and is intimately attached to the internal urinary sphincter through the neck (Miftahof & Nam, 2013). The neck is the funnel-shaped extension of the body (Miftahof & Nam, 2013).
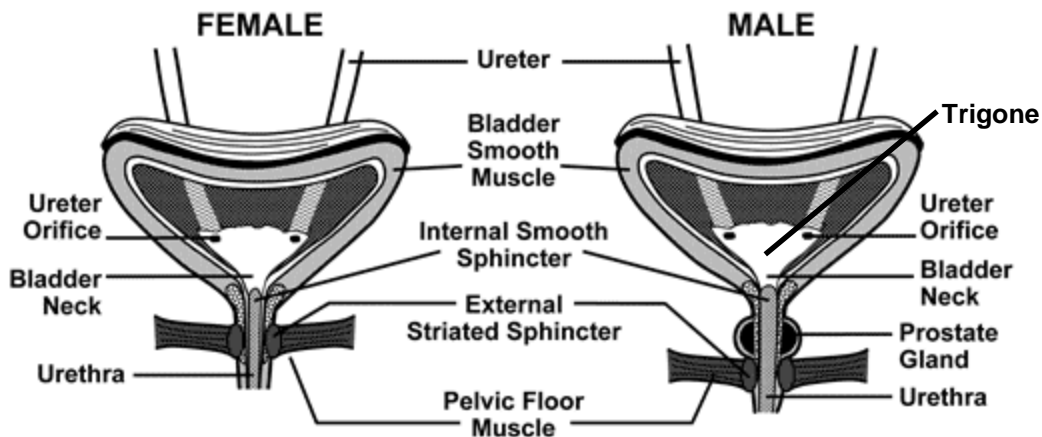
Fig. 1.1 Anatomical divisions of the human urinary bladder (Reproduced and modified from seek wellness, *Urinary bladder and kidneys – how they works*, by Newman, January 2002, retrieved from http://www.seekwellness.com).

1.3. Bladder wall tension and pressure

Clinical urodynamic testes quantify the pressure-volume relationships during filling, but do not measure bladder wall tension. These tests are used to assess detrusor activity, sensation, capacity, and compliance. Urodynamics (or cystometry) includes the study urine flow in the bladder, the urinary sphincter, and the urethra (Miftahof & Nam, 2013). Rose first studied and reported the cystometric technique in 1927 (Rose, 1927) and it has been extensively used since then for both

research and clinical purposes. Today, urodynamic investigations remain "the gold standard" (Miftahof & Nam, 2013), and researchers conduct a series of tests which employ the real time monitoring of changes in abdominal pressure (P_{abd}), vessel pressure (P_{ves}), and bladder capacity during the filling phase of the bladder (Andersson & Arner, 2004). Cumulative bladder capacity and detrusor pressure ($P_{det} = P_{abd} - P_{ves}$) are calculated using the data acquired from a urethral catheter with a pressure transducer and a rectal pressure transducer (Miftahof & Nam, 2013). These calculations provide valuable quantitative information about the overall behavior of the bladder, and are employed in the evaluation of the functionality of the bladder.
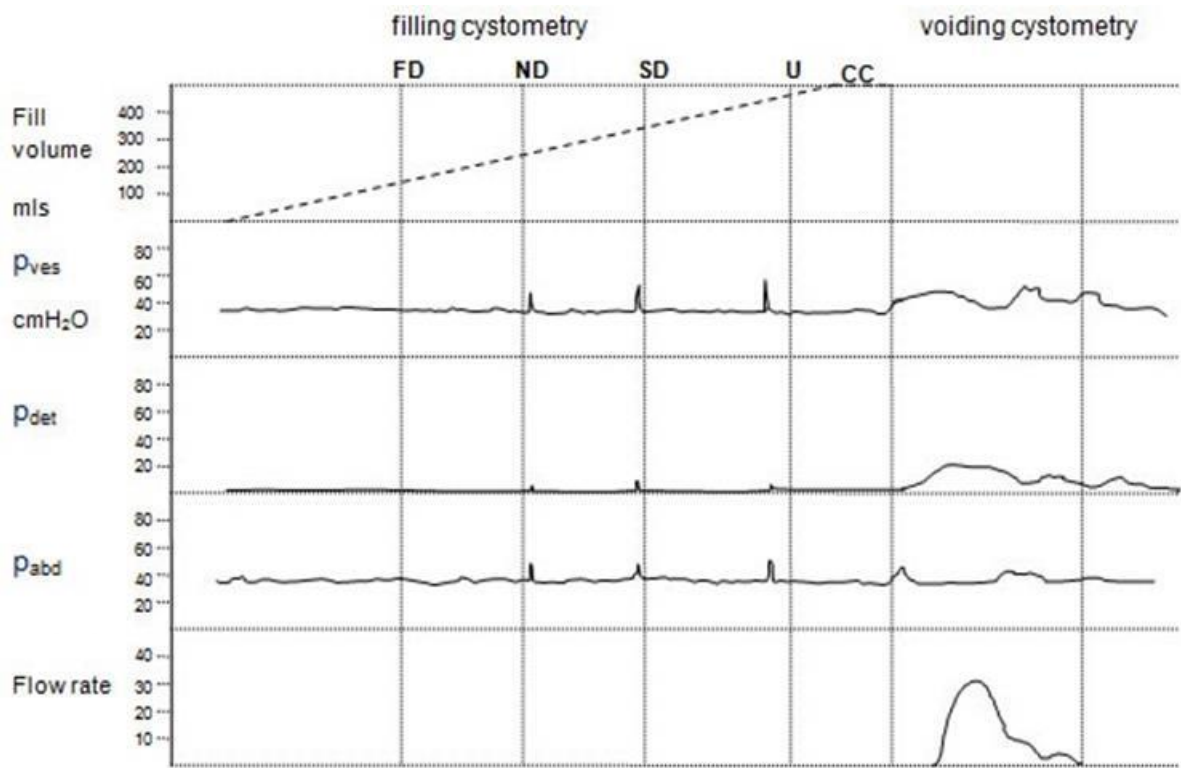
Fig. 1.2 A 48 year's old female normal human bladder filling Cytometery. FD (first desire to void); ND (normal desire to void); SD (strong desire to void); U (urgency); CC (cystometric capacity or permission to void given) (Reproduced from Bladder Urogynaecology Prolapse, *Bladder filling cytometery,* by Bernard T. Haylen, 2014, retrieved from http://www.bladder.com/glossary).

From the Fig. 1.2 above the detrusor pressure is relatively constant or low throughout the filling regardless of the volume. The filling detrusor pressure increase does not usually exceed 5—10

cm-H_2O (Frenkl et al., 2011) due to the viscoelastic properties of the bladder. P_{det} remains low until the voluntary voiding phase as in Fig. 1.2. Rises in P_{det} may be caused by involuntary detrusor contractions coughing, sneezing and/or impaired compliance.

Tension-sensitive nerves in the bladder wall provide fullness information that is interpreted as urgency (Kanai & Andersson, 2013). Bladder wall tension, and therefore nerve output, is a function of bladder volume, wall compliance and shape. Clinical urodynamics studies are used to quantify the pressure-volume relationship throughout filling with a catheter and the overall bladder compliance (Δvolume/Δpressure) for a particular fill (Mahfouz et al., 2012); however, these studies often reveal only small increases in filling phase pressures (Frenkl et al., 2011) in patients with or without heightened urgency. These standard pressure measurements do not necessarily reflect the underlying wall tension, which may correlate better with urgency.

The bladder wall undergoes large changes in extension during normal filling and emptying (Andersson & Arner, 2004). The increase of stress due to the stiff collagen fibers cause a small increase in pressure resulting during cystometry. These collagen fibers are kinked and coiled when the bladder is relaxed and begin to stretch during filling (Korkmaz & Rogg, 2007). Isolated strips of the bladder wall can be examined *in vitro* to determine the relation between length and wall tension. These data for the relation between length and force can be converted to volume and pressure data using the law of Laplace and assuming a model for the bladder shape and for how the wall stretch is distributed in the bladder wall. An assumption of spherical bladder shape, with an incompressible wall and isometric homogenous stretch, can give a good description of the bladder mechanics during filling (Andersson & Arner, 2004).

The first objective of this thesis is to use relatively simple physical and mathematical models to demonstrate that wall tension and stress (tension/cross-sectional area) can vary significantly with geometry in a vessel with uniform internal pressure. This will provide motivation for the investigation of a potential correlation between bladder wall stress parameters and patient-reported fullness sensations throughout bladder filling.

1.4. Bladder smooth muscle

Muscles are the contractile tissues of the body. They relax and contract to generate force for a particular movement. There are three types of muscles; skeletal, cardiac, and smooth muscle. Skeletal muscle is voluntary muscle mounted to the bone which supports skeletal movement during locomotion and in maintaining posture. Cardiac muscle is involuntary muscle found only in the heart. Like cardiac muscle, smooth muscle is involuntary muscle. Smooth muscle is non-striated muscle located in the walls of hollow structures and organs such as urinary bladder, esophagus, stomach, and uterus. Smooth muscle cells are not striated, which means the myofibrils are not arranged in easily distinguished sarcomeres. Smooth muscle in the urinary bladder is called detrusor smooth muscle (**DSM**).

Smooth muscle tissues are small and tapered-with the ends reducing in size, in contrast with the cylindrical shape of skeletal muscle. Each smooth muscle tissue has a single centrally located nucleus. The cells range in size from 5 to 10 µm in diameter in the center of the cell and from 300 to 600 µm in length (Miftahof & Nam, 2013). A substantial portion of the volume of the cytoplasm of smooth muscle cell is taken up by the molecules myosin and actin. Myosin is a motor protein and actin is either a globular or filamentous protein. The filamentous actin interacts with myosin (Schwartz & Mecham, 1995). Myosin lever arms pull on actin filaments to shorten the muscle cells and contract the tissue.

The process of muscle shortening can be explained in the following stages:

a. Myosin head attaches to actin (high energy **ADP** + P configuration) forming a cross-bridge.
b. Power stroke: myosin head pivots pulling the actin filament toward the center.
c. The cross-bridge detaches when a new ATP binds with the myosin.
d. Cocking of the myosin head occurs when **ATP** → ADP + P so another cross-bridge can form.

The various motor neurons to a whole muscle fire asynchronously. While some motor units are active others are inactive. This pattern of activity prevents muscle fatigue and produces smooth movements.

1.5. Regulated bladder compliance

Strips of rabbit detrusor smooth muscle exhibits regulated bladder compliance characterized by strain softening: a loss of stiffness on a stretch to a new length distinct from viscoelastic behavior (Speich et al., 2006). Several studies have demonstrated that repeated stretches of "passive" rabbit or mouse bladder strips (Ratz & Speich, 2010; Speich et al., 2006; Speich, Borgsmiller, Call, Mohr, & Ratz, 2005) or repeated filling of isolated mouse bladders (Speich et al., 2012) can strain-soften or increase the compliance of the bladder (Almasri, Ratz, & Speich, 2010; Speich et al., 2006; Speich, Almasri, Bhatia, Klausner, & Ratz, 2009; Speich et al., 2005; Speich et al., 2007), just as repeated stretches of a latex balloon make it easier to inflate. Moreover, unlike a latex balloon, an increase in compliance due to strain softening can be reversed by active contraction at short muscle lengths (Almasri, Ratz, Bhatia, Klausner, & Speich, 2010; Speich et al., 2006, 2009, 2005; Speich et al., 2007). Thus, bladder wall compliance is strain-history-dependent and activation-history-dependent. Most importantly, the change in regulated compliance associated with repeated passive filling is greater in a partial bladder outlet obstructed (**PBOO**) mouse model of detrusor overactivity (Speich et al., 2012). This preclinical data provides evidence that detrusor overactivity, and potentially overactive bladder in humans, may be associated with regulated compliance. The second objective of the present study, is to use published experimental data (Speich et al., 2007) to determine ranges for regulated detrusor compliance and to expand a finite deformation model of bladder filling to illustrate the potential effects of acute regulation of compliance on filling pressure and wall stress (Janz, Kubert, Pate, & Moriarty, 1980; Saito & Oki, 1982; Watanabe et al., 1981).

1.6. Bladder shape

Normal bladders vary in shape as shown in Fig. 1.3 (Zhang, Wu, Xi, Wang, & Jiang, 2012), and bladder compliance has been shown to depend on shape (Margot S Damaser & Lehman, 1993; Margot S. Damaser & Lehman, 1995). Ultrasonic estimation of bladder volume can be affected by the variations in bladder shape (Bih, Ho, Tsai, Lai, & Chow, 1998).

For a vessel containing a given volume of liquid, the shape with the smallest surface area is a sphere. Thus, any clinically observed condition that makes a normally spherical bladder less

spherical (e.g. pregnancy (van Brummen, Bruinse, van de Pol, Heintz, & van der Vaart, 2006), obesity (Chancellor, Oefelein, & Vasavada, 2010), or constipation (Kim, Lee, Jung, & Lee, 2011)) increases surface area, and therefore could increase the strain on tension-sensitive nerves, leading to an overestimate of bladder fullness for a given volume and urgency. One objective of this thesis is to develop a simple geometric model to examine the potential effect of bladder shape and constrained filling on wall tension and fullness sensation.

Different stimuli, such as position (lying or sitting) can lead to urgency. Stand up urgency (**SUU**) caused by a change in position, could be related to detrusor overactivity. Other causes to SUU may be the insufficiency of sphincter and urethral closure mechanisms (Hubeaux et al., 2012), which could be affected by pressure changes due to deformation of the bladder upon standing. As part of this thesis, a bladder deformation model will be developed to examine the increased pressure and wall tension caused by bladder deformation.
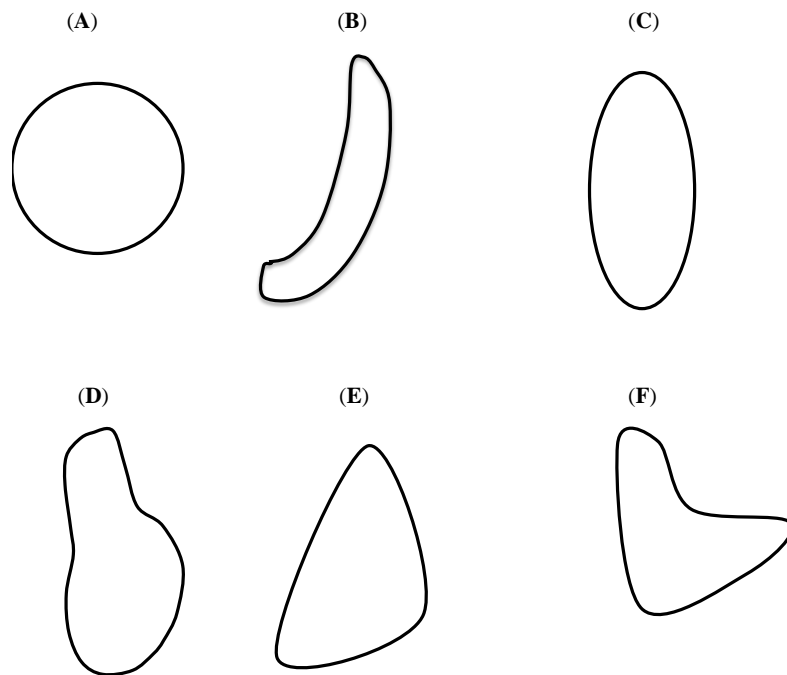
Fig. 1.3 Schematic diagram of bladder shapes: (A) sphere-shaped; (B) banana-shaped; (C)oval-shaped ; (D) pear-shaped; (E) triangular-shaped; (F)irregular-shaped (Zhang et al., 2012).

1.7. Thesis objectives

The first objective of this thesis is to develop relatively simple physical and mathematical models to demonstrate that wall tension and stress (tension/cross-sectional area) can vary significantly with geometry in a vessel with uniform internal pressure, and therefore motivate the investigation of a potential correlation between bladder wall stress parameters and patient-reported fullness sensations throughout bladder filling. (Chapter 2)

The second objective of this thesis is to use published experimental data (Speich, Dosier et al. 2007) to determine ranges for regulated detrusor compliance and to expand a finite deformation model of bladder filling (Janz et al., 1980; Saito & Oki, 1982; Watanabe et al., 1981) to illustrate the potential effects of acute regulation of compliance on filling pressure and wall stress. (Chapter 3)

The third objective of this thesis is to develop models to demonstrate that changes in bladder shape due to changes in compliance or intra-abdominal forces could contribute to changes in wall tension for a given volume that could lead to urgency. (Chapter 4)

The fourth objective of this thesis is to further study the change in bladder shape using a three-ring spheroidal bladder model to examine pressure and wall tension changes during deformation. (Chapter 5)

Chapter Two: Pressure and wall tension during bladder filling

2.1. Significance of bladder wall tension during filling

Bladder fullness information that is interpreted as urgency is provided by tension-sensitive nerves in the bladder wall (Kanai & Andersson, 2013). Bladder wall tension, and therefore nerve output, is a function of bladder volume, wall compliance and shape. Clinical urodynamics studies are used to quantify the pressure-volume relationship throughout filling with a catheter and the overall bladder compliance (Δvolume/Δpressure) for a particular fill (Mahfouz et al., 2012); however, these studies often reveal only small increases in filling phase pressures (Frenkl et al., 2011) in patients with or without heightened urgency. These standard pressure measurements do not necessarily reflect the underlying wall tension, which may correlate better with urgency. The first objective of this thesis is to use relatively simple physical and mathematical models to demonstrate that wall tension and stress (tension/cross-sectional area) can vary significantly with geometry in a vessel with uniform internal pressure. This will motivate the investigation of a potential correlation between bladder wall stress parameters and patient-reported fullness sensations throughout bladder filling.

2.2. Laplace's Law

Pascal's principle requires that the pressure is the same everywhere inside a balloon at equilibrium. However, experiments reveal that there are great differences in wall tension on different parts of a balloon. The variation is described by Laplace's Law. The larger the vessel radius, the greater the wall tension required to withstand a given internal fluid pressure.

According to Laplace's Law, the wall tension, T, in a thin-walled fluid-filled cylindrical or spherical vessel with homogeneous isotropic material properties is proportional to the product of the uniform internal pressure, P, and the radius of the vessel, R (Chancellor, Rivas, & Bourgeois, 1996; Fata et al., n.d.; Watanabe et al., 1981):

$$T \propto P \cdot R \qquad\qquad\qquad 2.1$$

In addition, the wall stress, σ, in a thin-walled spherical vessel with a uniform wall thickness, t, can be calculated using the following equation (Hibbeler, 2011).

$$\sigma = \frac{P \cdot R}{2t} \qquad\qquad 2.2$$

The thin wall assumption is typically used for vessels with a wall thickness of less than one-tenth of the vessel radius (t < R/10) (Hibbeler, 2011).

2.3. Demonstration of Laplace's Law using a rubber balloon

A typical cylindrical rubber balloon (Fig. 2.1A, Qualatex.com) was used to demonstrate Laplace's Law. The air in the relaxed balloon was removed by completely displacing it with water. Then, the balloon was partially filled with ~120 ml of water using a large syringe and the opening was sealed by tying the end of the balloon into a knot (Fig. 2.1B). Later, the balloon was manually squeezed to displace the bolus of water to different regions of the balloon (Fig. 2.1C-D) and then to divide the bolus into two roughly equal parts (Fig. 2.1E). The balloon was manually bent at the smaller radius between the divided bolus and released to an equilibrium position (Fig. 2.1F) and subsequently bent near the center of a single bolus and released to a second equilibrium position (Fig. 2.1G).

The balloon experiment in this chapter demonstrates that for a given fill volume, stress at a particular area can change; this indicates the potential for a change in stress measured by tension-sensitive nerves on the wall of the bladder without a change in volume. This example also demonstrated that external applied energy can create different stress points along the cylindrical balloon. This may imply an external deformation force applied to the bladder to change the shape and further increase the wall stress and nerve output at particular locations of the bladder.
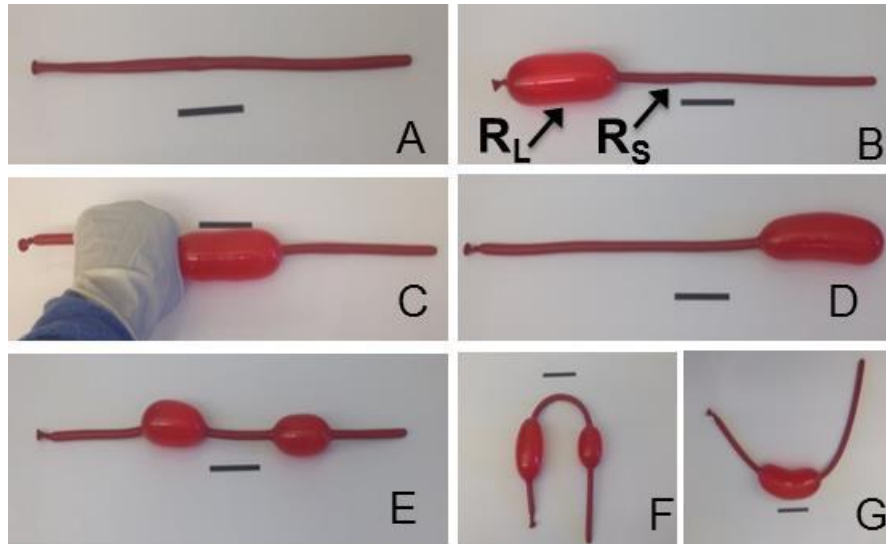
Fig. 2.1 Photographs of a rubber balloon demonstration. (**A**) An open, cylindrical, relaxed red balloon and a 5 cm black scale bar. (**B**) The balloon at equilibrium after ~120 ml of water was added and the balloon opening was sealed. Internal pressure was constant throughout the balloon; however, one region had a larger radius (R_L) and another region had a smaller radius (R_S). (**C**) The balloon was squeezed to provide energy to move the water to another region. (**D-E**) Other equilibrium positions showing that the region with the greater R_L was relocated by transient external forces. (**F**) The region with R_s was easily bent and remained bent when released. (**G**) The region with R_L required greater effort to bend and did not remain bent when released.

Chapter Three: Modeling the effect of regulated bladder compliance on bladder filling

3.1. Acute regulation of bladder compliance

Several studies have demonstrated that repeated stretches of "passive" rabbit or mouse bladder strips (Ratz & Speich, 2010; Speich et al., 2006, 2005) or repeated filling of isolated mouse bladders (Speich et al., 2012) can strain-soften or increase the compliance of the bladder (Speich, Borgsmiller et al. 2005, Speich, Quintero et al. 2006, Speich, Dosier et al. 2007, Speich, Almasri et al. 2009, Almasri, Ratz et al. 2010), just as repeated stretches of a latex balloon make it easier to inflate. Moreover, unlike a latex balloon, an increase in compliance due to strain softening can be reversed by active contraction at short muscle lengths (Speich, Borgsmiller et al. 2005, Speich, Quintero et al. 2006, Speich, Dosier et al. 2007, Speich, Almasri et al. 2009, Almasri, Ratz et al. 2010). Thus, bladder wall compliance is strain-history-dependent and activation-history-dependent. Most importantly, the change in regulated compliance associated with repeated passive filling is greater in a partial bladder outlet obstructed (**PBOO**) mouse model of detrusor overactivity (Speich et al., 2012). This preclinical data provides evidence that detrusor overactivity, and potentially overactive bladder in humans, may be associated with regulated compliance. The second objective of this thesis, is to use published experimental data (Speich, Dosier et al. 2007) to determine ranges for regulated detrusor compliance and to expand a finite deformation model of bladder filling to (Janz et al., 1980; Saito & Oki, 1982; Watanabe et al., 1981) illustrate the potential effects of acute regulation of compliance on filling pressure and wall stress.

3.2 Hyperelastic Materials

Elasticity is the tendency of solid materials to return to their original shape and size after being deformed by application of a force. Linear elastic models do not accurately describe the observed material behavior for many materials (Muhr, 2005). For example, the stress-stain relationship for material such as, rubber can be defined as nonlinear, isotropic, and incompressible. In this thesis, the stress-strain relationship for the model is derived by assuming the bladder is made of an incompressible, isotropic, and hyperelastic material like a rubber.

This kind of material is considered a hyperelastic continuum with a strain energy density function W represented by a scalar valued function of deformation gradient F. W can be represented in terms of the three invariants I_1, I_2, and I_3 which are defined through the principal stretches (strains) $\lambda_1, \lambda_2,$ and λ_3 for isotropic materials (Bechir, Chevalier, Chaouche, & Boufala, 2006). It is possible to assume that the material is incompressible when the material is not subjected to too large hydrostatic loadings and $I_3 = 1$ for incompressible materials. For such materials Valanis and Landel (1967) have proposed a simple form of the strain energy density W which is separable symmetric function of the stretches; $W = w(\lambda_1) + w(\lambda_2) + w(\lambda_3)$ (Valanis, 1967) and the principal stresses in the material can be obtained by taking the derivative of W with respect to the strains, λ_i. Equations 3.1 and 3.2 in the following section were derived using this simple approach.

3.3. Continuum model for regulated detrusor compliance

Watanabe *et, al.*, used finite deformation theory to develop a hyperelastic continuum model for the bladder, which was assumed to be spherical and made of an isotropic incompressible material (Janz et al., 1980; Saito & Oki, 1982; Watanabe et al., 1981). For uniaxial extension, the relationship between uniaxial stress σ_1, and the uniaxial extension ratio (strain) λ_1, was given by the equation:

$$\sigma_1 = a\lambda_1(\lambda_1 - 1)^{(b-1)} + \frac{a}{\sqrt{\lambda_1}}\left(1 - \frac{1}{\sqrt{\lambda_1}}\right)^{(b-1)} \qquad 3.1$$

Constant material property parameters **a** and **b** were determined by fitting this equation to data from a uniaxial length-tension experiment performed on strips of canine bladder (Watanabe et al., 1981). For spherical bladder filling, the relationship between wall stress, σ, the extension ratio of the bladder radius (strain), λ, and the material property parameters, a and b, was given by the equation:

$$\sigma = a\lambda(\lambda - 1)^{(b-1)} + \frac{a}{\lambda^2}\left(1 - \frac{1}{\lambda^2}\right)^{(b-1)} \qquad 3.2$$

In addition, bladder filling pressure, P, was defined as a function of wall stress; bladder mass, m; bladder density, ρ; and volume, V, using the equation:

$$P = \frac{2m\sigma}{3\rho V} \qquad\qquad 3.3$$

This model produced a relatively flat pressure-volume curve, as typically observed in a clinical cystometery (Mahfouz et al., 2012; Rose, 1927), and a wall stress curve that continued to rise with increasing volume.

For this thesis, equations 3.1—3.3 were used to predict the effect of acutely regulated detrusor compliance on filling pressures and wall stresses. First, uniaxial length-tension data from a previous study revealing regulated detrusor compliance in rabbit detrusor strips (Speich, Dosier et al. 2007) was converted to stress-strain data (Fig. 3.1A) using an estimated undeformed cross-sectional area of 0.9 mm^2 (Speich et al., 2007). Next, the first ten data points of the ascending or lower compliance curve (**LCC**) were fit to a linear curve, and this line was extrapolated to estimate the point of zero stress and a strain ratio of one (Fig. 3.1B). Then, equation 3.1 was fit separately to the lower compliance curve and the higher compliance (descending) curve (**HCC**) to determine the range or the constant material property parameters *a* and *b* for the range of regulated detrusor compliance revealed in this particular experiment. The curve fit was done using Graphpad Prism 6.0 software and the best-fit values for the lower compliance curve were; *a* = 0.1242 N/cm^2 and *b* = 4.066 with standard error of 0.009513 and 0.09050 respectively. Likewise the higher compliance curve had values of *a* = 0.000001138 N/cm^2 and *b* = 16.06 with standard error of 1.264x10^{-6} and 1.236 respectively. A change in the value of *a* will shift the magnitude of the stress at each strain. The constant *b* is the exponent in equation 3.1 and a change in the value will affect the curvature of the curve fit in Fig. 3.1.
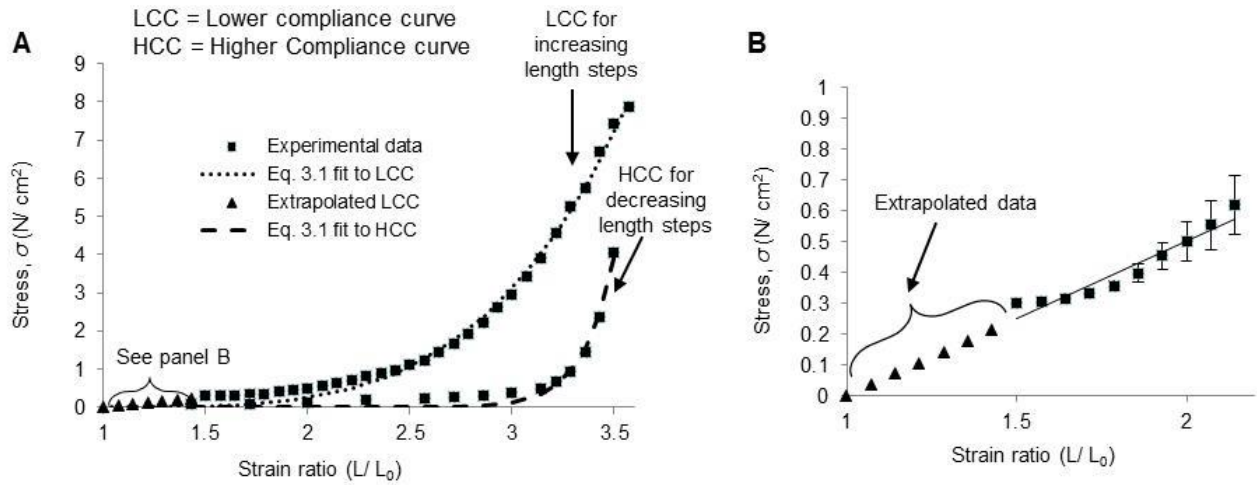
Fig. 3.1 (**A**) Stress-strain curves calculated from previously published uniaxial tension-strain curves for rabbit DSM strips (solid symbols) illustrating an acute change in this material property relationship due to regulated bladder compliance (**RBC**). Pseudo-steady-steady state stress measured at each length during a sequence of increasing length steps (pre-strain softening, maximal RBC, **LCC**) was typically much greater than stress at the same length during a subsequent set of decreasing length steps (post-strain softening, minimal RBC, **HCC**) due to RBC (Speich et al., 2007). (**B**) The LCC was extrapolated to a strain ratio of one using a linear fit to the first ten data points of the LCC. Then, the stress-strain equation (equation 3.1) for the finite deformation model was fit separately to the LCC and HCC (**A**).

Pressure-volume curves and wall-stress-volume curves (Fig. 3.2) were produced using equations 3.2 and 3.3 for a volume range for a rabbit of 2-90 ml (Matsumoto, Chichester, Bratslavsky, Kogan, & Levin, 2002). Bladder density and mass were estimated to be 1.05 gm/cm^3 and 2.5 gm, respectively, as in previous studies (Speich et al., 2007). Wall thickness, t, was calculated using the relationship:

$$t = \frac{m}{4\rho\pi r^2}$$
3.4
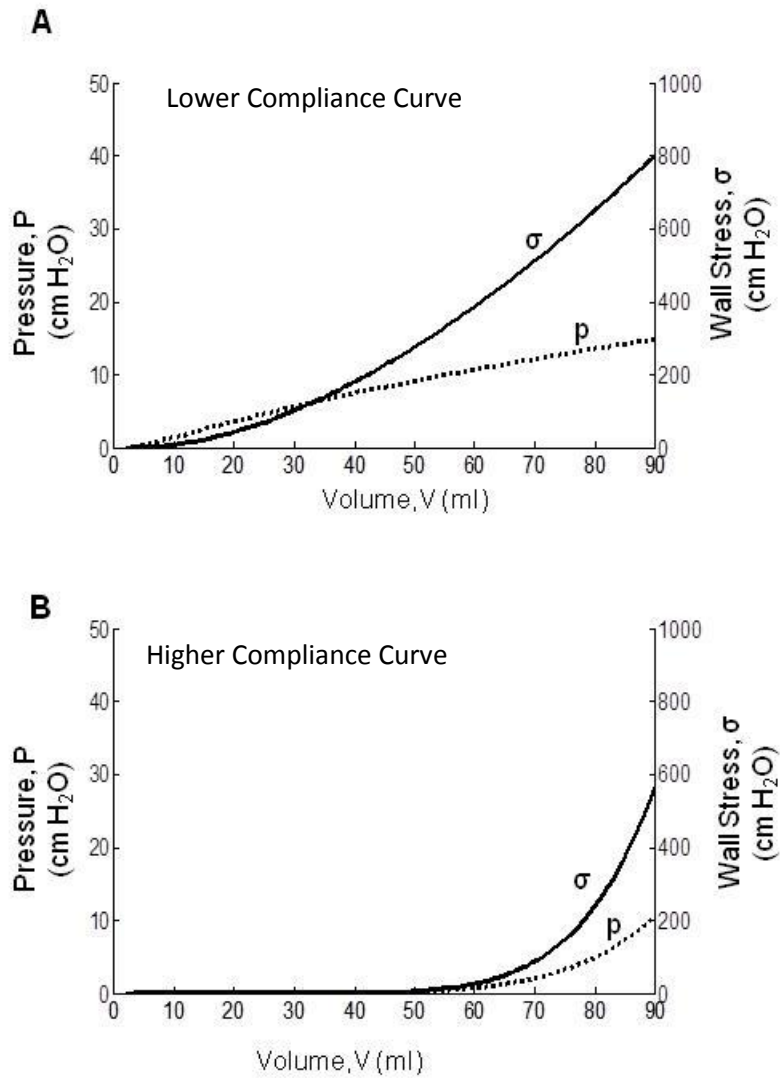
Fig. 3.2 Pressure-volume and stress-volume curves for rabbit DSM with (**A**) lower regulated bladder compliance (pre-strain softening, lower compliance curve in Fig. 3.1) and with (**B**) higher regulated bladder compliance (post-strain softening, higher compliance curve in Fig. 3.1) corresponding to the data calculation from Fig. 3.1 for pressure and stress for LCC (**A**) and HCC (**B**).
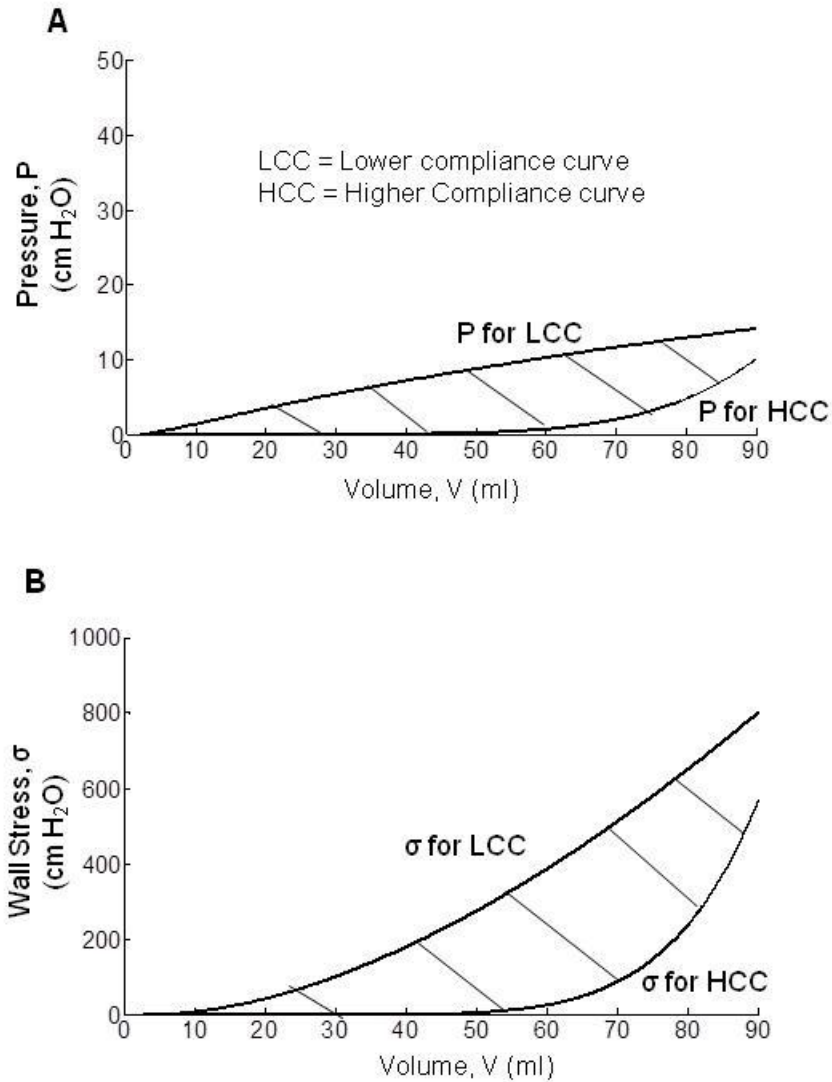
Fig. 3.3 Pressure-volume curves (**A**) and stress-volume curves (**B**) corresponding to the LCC and HCC. Shaded areas show ranges of pressure (**A**) and wall stress (**B**) permitted by regulated detrusor compliance.

From Fig. 3.3 it is possible to observe the changes in pressure and stress associated with the acutely regulated changes in compliance due to adjustable preload stiffness in Fig. 3.1.

For comparison, wall stress was also calculated using equation 3.3 for a bladder with a constant pressure of 14.14 cm-H_2O (Fig. 3.4) corresponding to the maximum pressure in Fig. 3.2A. According to equation 3.3, if pressure is constant, the stress and volume will have linear relationship as shown in Fig. 3.4B. This example demonstrates that wall stress increases significantly even if filling pressure remains constant.
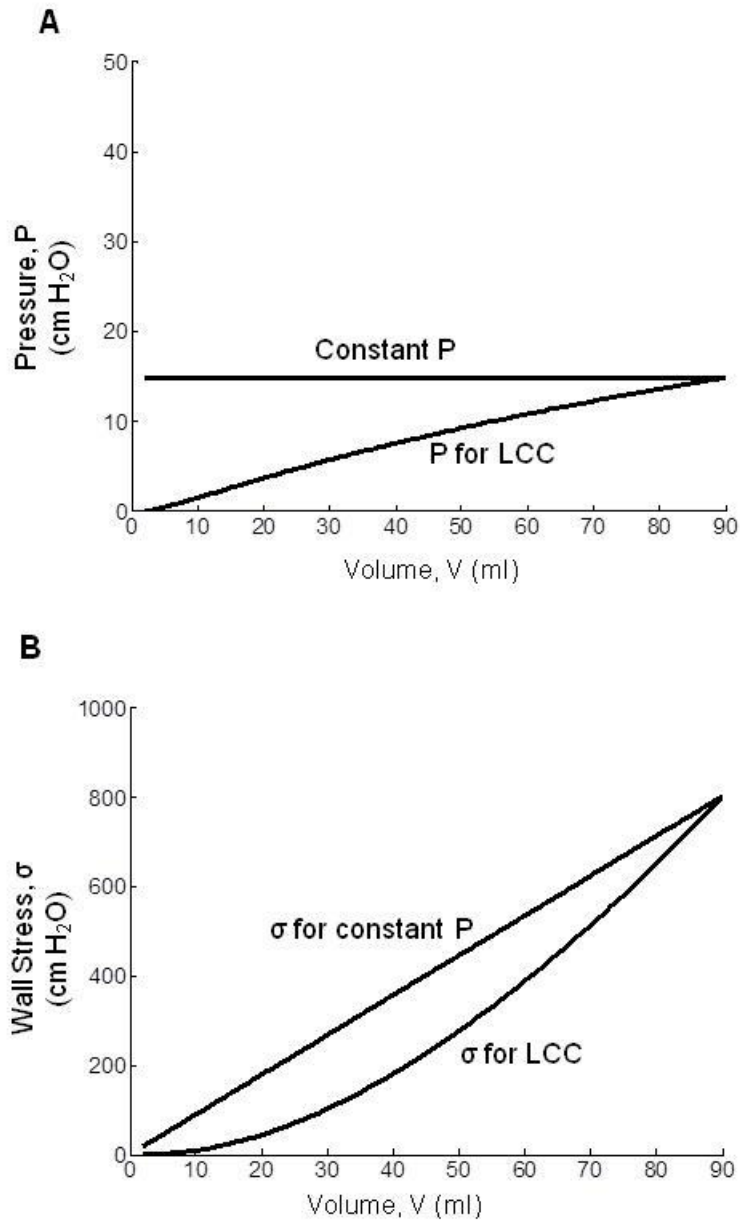
Fig. 3.4 Pressures (**A**) and corresponding wall stresses (**B**) for the lower compliance curve from Fig. 3.1 and for a constant pressure of 14.14 cm-H_2O.

Generally, the model results in this chapter show that as the volume increases the pressure shows relatively a small change whereas the wall stress is significantly increasing. Furthermore, a finite deformation continuum model is compared with a constant pressure model. Choosing an appropriate model which approximates the experimental data and the clinical measurements to describe the behavior of the bladder is very important.

Chapter Four: Modeling the effect of a change in bladder shape

4.1. Importance of bladder shape change during filling

Normal bladders vary in shape, and bladder compliance has been shown to depend on shape (M S Damaser & Lehman, 1993; Margot S. Damaser & Lehman, 1995). For a vessel containing a given volume of liquid, the shape with the smallest surface area is a sphere. Thus, any clinically observed condition that makes a normally spherical bladder less spherical (e.g. pregnancy (van Brummen et al., 2006), obesity (Chancellor et al., 2010), or constipation (Kim et al., 2011)) increases surface area, and therefore could increase the strain on tension-sensitive nerves, leading to an overestimate of bladder fullness for a given volume and urgency. One objective of this thesis is to develop a simple geometric model to examine the potential effect of bladder shape and constrained filling on wall tension and fullness sensation.

The filling pressure-volume curve of the urinary bladder is called cystometrogram (**CMG**), and is measured by increasing the contained volume and measuring the pressure response. The CMG depends on the constitutive properties of the bladder tissue and the wall thickness. Mathematical models have been developed by researchers to infer material constitutive properties from whole bladder properties. Most existing models assume isotropy, homogeneity and incompressibility of the bladder wall material (M S Damaser & Lehman, 1993; Margot S. Damaser & Lehman, 1995). In this chapter, a model will be developed to show the potential importance of bladder shape.

4.2. Model for bladder shape change

Mathematical models of the urinary bladder are used to obtain material parameters, such as stress and strain, from measurable whole bladder parameters, such as pressure and volume. Because of its mathematical simplicity, spherical model of the bladder has been used (M S Damaser & Lehman, 1993; Margot S. Damaser & Lehman, 1995). However, normal bladders vary considerably in their shape (M S Damaser & Lehman, 1993; Margot S. Damaser & Lehman, 1995). In this chapter a model is developed to investigate shape change, keeping material properties constant.

A spheroidal geometric model was used demonstrate the potential effect of bladder shape change on bladder wall stress (Fig. 4.1). The volume, V, of a spheroid is a function of the three principal axis radii, R_1, R_2 and R_3 as given by the equation:

$$V = \frac{4}{3}\pi R_1 R_2 R_3 \qquad\qquad 4.1$$
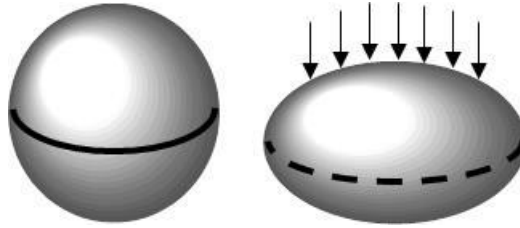
Fig. 4.1 A spherical bladder (left) and a bladder constrained (arrows) in one radial direction to form an oblate spheroid (right). Both have equatorial wall strips equal to one half of the circumference (solid and dashed lines, respectively).

For a perfectly spherical bladder, the radii are equal ($R_1 = R_2 = R_3$). However, if the spheroidal bladder is externally constrained such that two radii, R_2 and R_3, are a fraction, β, of the other radius ($R_1 = \beta R_2 = \beta R_3$), then the bladder fills as an oblate sphere (Fig. 4.1) (M S Damaser & Lehman, 1993; Margot S. Damaser & Lehman, 1995). For both the perfect and oblate spheroids, the largest radius for each volume, R_{max}, is defined by the equation:

$$R_{max} = \sqrt[3]{\frac{3V}{4\beta\pi}} \qquad\qquad 4.2$$

In this equation, $\beta = 1$ for the perfect sphere and $\beta < 1$ for the oblate sphere. The oblate spheroid has one circular cross-section with radius R_1 and two ellipsoidal cross-sections, one with radii R_1 & R_2 and the other with radii R_1 & R_3. As β decreases from 1.0, the radius of the circular cross-section R_1 increases and the other radii R_2 and R_3 decrease.

For each spheroid model, a detrusor strip along the largest circumference was examined (Fig. 4.1), and the length of this strip was defined as half of the largest circumference using the equation:

$$L = \frac{1}{2} 2\pi R_{max} = \sqrt[3]{\frac{3V\pi^2}{4\beta}}$$ 4.3

A

B
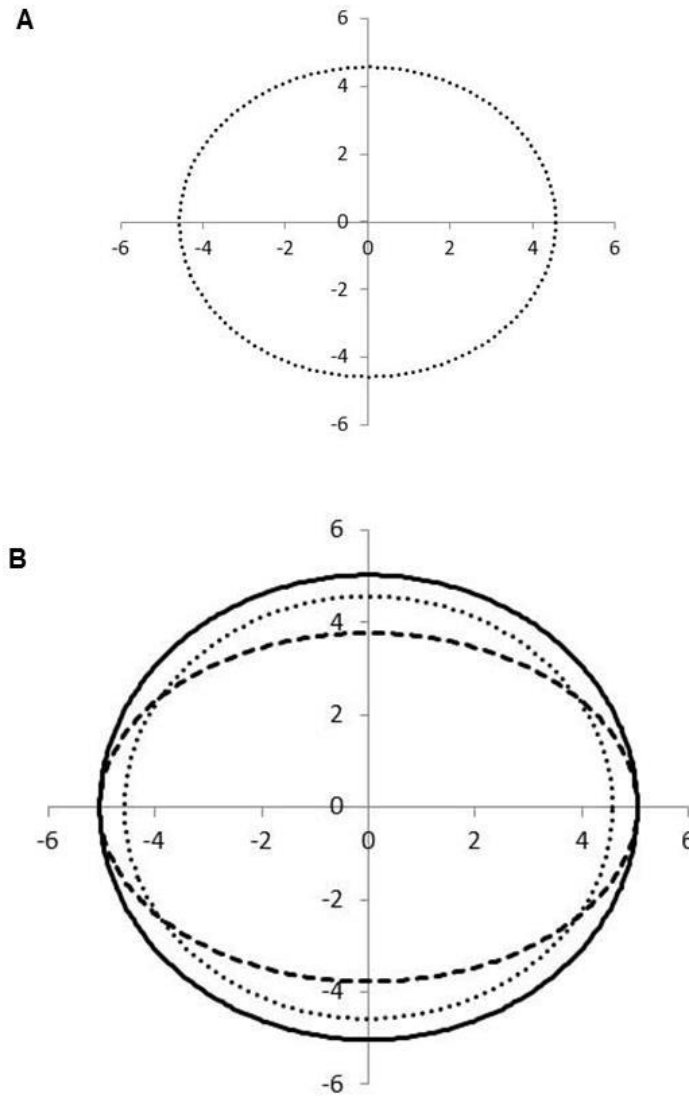
Fig. 4.2 The circular circumference for a sphere with a volume of 400 ml is identical for the top, side and front views (**A**). An oblate spheroid with the same volume and $\beta = 0.75$ has one circular cross-section (**B**, solid line, top view) and two identical ellipsoidal cross-sections (**B**, dashed line, front and side views). The larger radius of each of these cross-sectional views of the oblate

spheroid (**B**, solid and dashed lines) is greater than the radius of the circular cross-section of the sphere (**B**, dotted line).

As an example, a value of β = 0.75 was selected for the following oblate spheroid calculations. A spherical bladder is assumed to reach its micturition threshold at 400 ml with an equatorial wall strip length equal to ½ the circumference, or 14.36 cm (Fig. 4.1 solid line strip and Fig. 4.2 point **A**). If this bladder is constrained by 25% in one radial direction to form an oblate spheroid (Fig. 4.1 arrows), it reaches the same threshold strip length (14.36 cm) at only 300 ml (Fig. 4.1 dashed line strip, Fig. 4.2 point **B**). This example illustrates that a change in shape due to external constraints could substantially decrease the volume at which a person experiences a strong desire to void, which would lead to more frequent voiding.
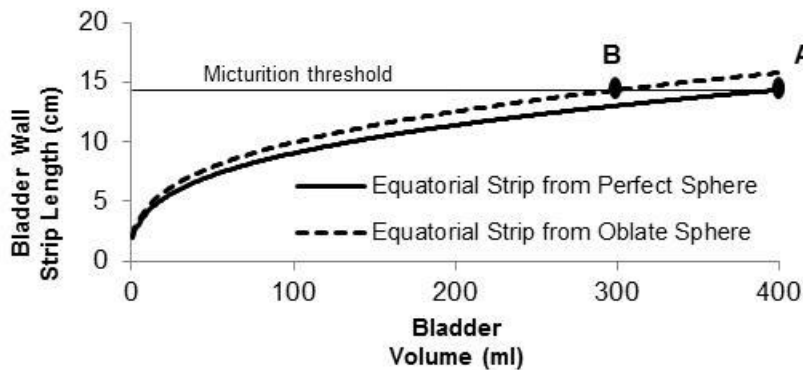
Fig. 4.3 Human bladder wall strip length during filling from 0 to 400 ml. A spherical bladder is assumed to reach its micturition threshold at 400 ml with an equatorial wall strip length equal to ½ the circumference, or 14.36 cm (point **A**). If the same bladder is constrained in one radial direction to form an oblate spheroid with β = 0.75, it reaches the same threshold strip length (14.36 cm) at only 300 ml (point **B**).

Chapter Five: Orthogonal Three-ring Spheroid Model for bladder shape change

Bladder tissue shows viscoelastic, non-linear behavior, and is non-isotropic and non-homogenous; therefore, studying the bladder's mechanical properties is extremely sophisticated (Fung, 1993; Korkmaz & Rogg, 2007; Miftahof & Nam, 2013). Bladder wall includes layers of muscle bundles arranged in particular directions (Fujii, Takagi, Arimoto, Ootani, & Ueeda, 2000). Strips or bundles from the bladder wall of animals can be excised and tested in a uniaxial tensile testing apparatus to characterize the mechanical properties and approximate the behavior of the urinary bladder during filling (Miftahof & Nam, 2013). In this chapter, a model with three orthogonal muscle rings (strips) was developed (Fig. 5.1). The three strips were assumed to support all the internal pressure and external forces acting on the bladder. Homogeneous bladder material, uniaxial loading in the circumferential direction, and stress-free lateral edges were assumed. The objective of this model is to predict the change in vessel pressure, wall tension and external deformation force required to uniaxially deform an isovolumetric spherical bladder into an oblate spheroid.

5.1. Development of an isovolumetric deformation model

The goal of this section is to give a mathematical model consisting of three equivalent bladder strips that overlap each other to form a sphere. The model will be used to predict the change in vessel pressure and external deformation force required to uniaxially deform an isovolumetric spherical bladder into an oblate spheroid and estimate the change in wall tension. In order to develop this mathematical model, a particular volume and the corresponding vessel pressure must be selected. These values can be arbitrarily selected, taken from another model, or taken from urodynamics test. In addition, uniaxial stress-strain data for the tissue (equation 3.1) is used to calculate the area of the strips. Model results such as, tension and stress for each strip, pressure increase upon deformation, and deformation force are displayed in the next section of this chapter.

The bladder was assumed to fill without any external forces applied as a sphere consisting of three equivalent orthogonal strips as shown in Fig. 5.1. The first step in the development of this model was to estimate the volume of the strips (volume of tissue) based on a particular fluid volume and vessel pressure. For the example in this chapter, a fluid volume of 60 ml and pressure of 10.25 cm-H_2O were used based on the rabbit bladder example in Fig. 3.4.
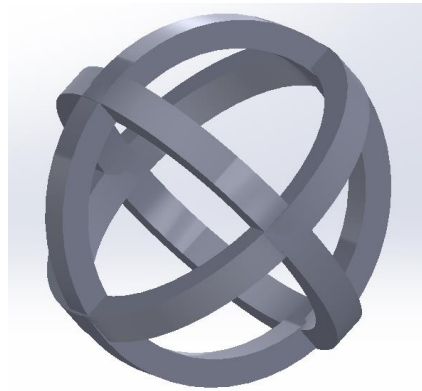
Fig. 5.1 Three equivalent rings representing a spherical bladder shape. (Note: rings overlapped each other).

Each ring was assumed to undergo uniaxial extension along its circumference and follow a relationship between strain and stress that can be evaluated from a uniaxial extension test using equation 3.1. From the geometry of a sphere, the area of the fluid cross-section, A_{fluid} ($A_{fluid} = \pi r^2$) and length of the strip, L_{strip} ($L_{strip} = 2\pi r$) can be evaluated (Fig. 5.2), where r is the radius of the sphere.

$$A_{fluid(c)} = \pi r_c{}^2$$

$$L_{strip(c)} = 2\pi r_c$$
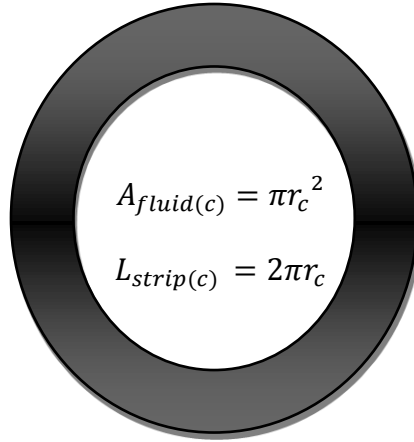
Fig. 5.2 Geometric analysis of the cross-sectional area of the fluid and the circumference (length) of the ring (strip) for the spherical model.

The sphere was cut to produce a hemisphere with two strips as indicated on Fig. 5.3. The pressure, *p,* inside the sphere is acting to force the strip-hemisphere in the upward direction (Fig 5.3). This total force must be the product of the pressure and the area of the imaginary circular plane formed by the strip hemisphere (Fig. 5.2). The upward total force, T, acting on the wall due to the pressure inside the fluid cross sectional area is calculated as:

$$T = p * A_{fluid(c)} \qquad\qquad 5.1$$

This total force must be balanced by the tension in the strips. The tension in each strip must be equal T/4 due to symmetry (Fig. 5.3). The uniaxial stress, σ, in the each strip can be calculated using equation 3.1 for the same material properties *a* and *b* (a = 0.1242 N/cm^2 and b = 4.066). The tension (Fig. 5.3 downward force) on the bladder wall will be:

$$\frac{T}{4} = \sigma * A_{strip} \qquad\qquad 5.2$$

The cross-sectional area of each strip A_{strip} can be computed using equations 5.1 and 5.2, then the volume of tissue in the three strips can be evaluated as:

$$V_{strips} = 3(A_{strip} * L_{strip}) \qquad\qquad 5.3$$

25

The constant coefficient 3 is to indicate that there are three equivalent strips holding the pressure. Now, the length, cross-sectional area and volume of each strip are known. This geometric information, along with the uniaxial stress-strain relationship (eq 3.1) will be used to examine bladder deformation in the following section.
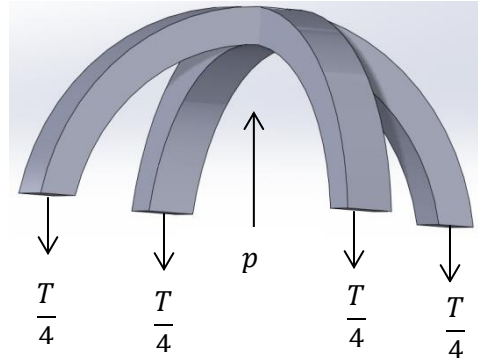
Fig. 5.3 Force analysis for the front view of the spherical strip model with a side-to-side cut with tension on the strips and the vertical force due to the vessel pressure.

4.2. Isovolumetric deformation model

The strip volume and fluid volume from the above model will be adopted here to develop an isovolumetric deformation model. This particular section focuses on the prediction of the change in vessel pressure and external deformation force required to uniaxially deform an isovolumetric spherical bladder into an oblate spheroid and estimate the change in wall tension.

A homogeneous isotropic strip membrane was deformed so that its eccentricity (deviation from circularity) changes, when an external force, F, is applied normal to the surface of the sphere in addition to the uniform hydrostatic pressure is applied to its interior surface. The force is assumed to deform the bladder from a sphere into a spheroid such that one radius, r_c, is a fraction, β, of the other two radii ($r_e = \beta r_c$) to form an oblate spheroid as described in Chapter 4. The model requires selection of a volume, pressure and a uniaxial stress-strain curve for a tissue strip and enables calculation of the change in pressure and stress and the deformation force necessary for a particular change in shape beta (β).

Fig. 5.4 An external perpendicular force F applied to deform the bladder and change the shape.

In this particular case the three strips will not have the same length because of the external deformation force, F applied on the wall as shown in Fig. 5.4. Assume the top view is a circle and the front and side views are ellipses and the volume of each strip is the same as calculated in equation 5..3 and as shown in Fig. 5.5. Assume the same volume of fluid V and tissue V_{strip} (i.e., the bladder is filled with the same amount of fluid for both sphere and oblate spheroid).

$$V = \frac{4}{3}\pi r^3 = \frac{4}{3}\pi r_1 r_2 r_3 = \frac{4}{3}\pi r_c r_e^2 \qquad\qquad 5.4$$

$$V_{strip} = V_{strip(c)} = V_{strip(e)} = \frac{V_{strips}}{3}$$

In equation 5.4, r is radius of the sphere, $r_1(r_c)$, $r_2(r_e)$, and $r_3(r_e)$ are radii of the oblate spheroid, and r_c and r_e stand for radius of circle and smaller radius of the ellipse respectively as shown in Fig 5.5. The deformation force exerted externally causes the principal radius to reduce in one direction and increase in the other direction, i.e., one radius is β fraction of the other, $r_e = \beta r_c$ and β is any fraction less than one and greater than zero. When β = 1 all the radii will be equal and the spheroid will be a perfect sphere. For the oblate spheroid, the length of the strip

27

is different for circle and ellipse, and the corresponding uniaxial stress is also varies. From equation 3.1, these uniaxial stresses for circular and ellipsoidal strips can be calculated as:

$$\sigma_c = a\lambda_c(\lambda_c - 1)^{(b-1)} + \frac{a}{\sqrt{\lambda_c}}\left(1 - \frac{1}{\sqrt{\lambda_c}}\right)^{(b-1)} \qquad 5.5$$

$$\sigma_e = a\lambda_e(\lambda_e - 1)^{(b-1)} + \frac{a}{\sqrt{\lambda_e}}\left(1 - \frac{1}{\sqrt{\lambda_e}}\right)^{(b-1)}$$

$$\lambda_e = \frac{L_{strip(c)}}{2\pi r_0}; \; \lambda_c = \frac{L_{strip(c)}}{2\pi r_0}$$

where $r_0 = \sqrt[3]{\frac{V_0}{4\pi}}$ is the initial fluid radius, which is calculated from the initial fluid volume of 2 cm^3, defined in Chapter 3, and λ_e and λ_c are extension ratios of the ellipsoidal and circular strips, respectively. From the geometry relationships, the cross-sectional area of the fluid and length of the strips for the circular and ellipsoidal regions can be determined.

$$A_{fluid(e)} = \pi r_e r_c; \; A_{fluid(c)} = \pi r_c^2 \qquad 5.6$$

$$L_{strip(c)} = 2\pi r_c$$

$$L_{strip(e)} = \pi[3(r_e + r_c) - \sqrt{(10r_c r_e) + 3(r_c^2 + r_e^2)}]$$

$L_{strip(e)}$ in equation 5.6 is the Ramanujan approximation for circumference of an ellipse (Villarino, 2005).
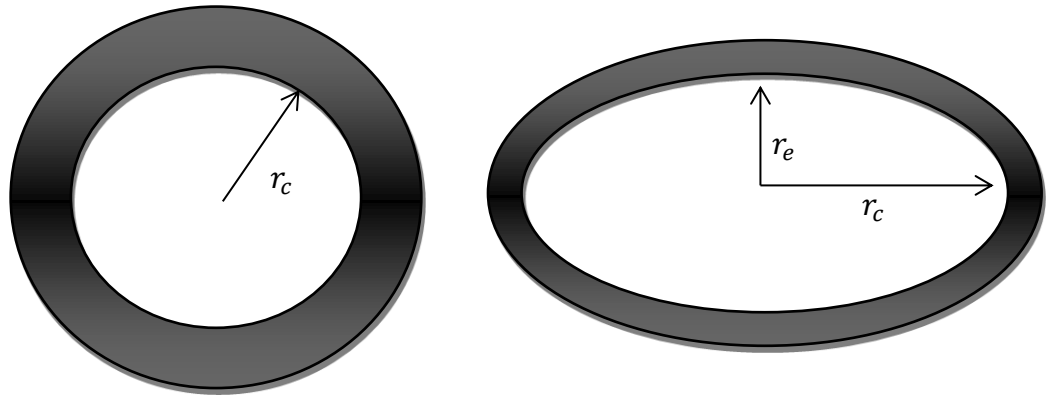
Fig. 5.5 Geometric of the cross-sections of the circular and elliptical planes of the oblate spheroid.

The cross-sectional area of each strip can be evaluated from the volume and length of each strip (equation 5.4 and 5.6) and given as:

$$A_{strip(c)} = \frac{V_{strip(c)}}{L_{strip(c)}}; \quad A_{strip(e)} = \frac{V_{strip(e)}}{L_{strip(e)}} \qquad 5.7$$
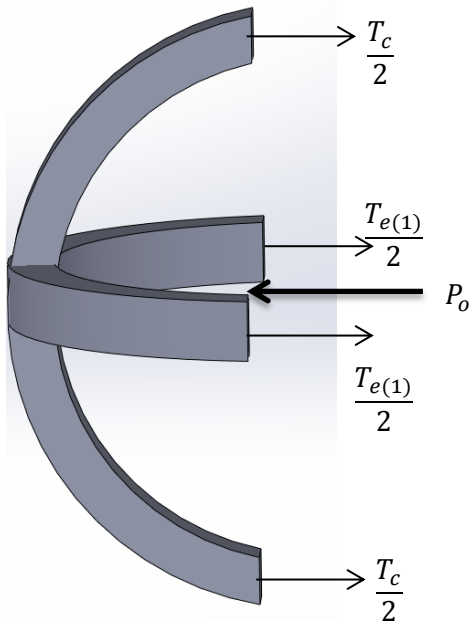
Fig. 5.6 Force analysis for the top view of the oblate spheroid model with a front–to-back midline cut through a circular strip and an ellipsoidal strip.

The pressure P_o inside the oblate spheroid is calculated using the hemisphere cut parallel to the external force. This total force due to the pressure must be the product of the pressure and the area of the circular plane formed by the hemisphere, i.e., $P_o. \pi r_c r_e$. This force must be balanced by the sum of the tensions on each end of the circular strip and each end of the ellipsoidal strip. The tension on the end of the circular strip is the product of the circular uniaxial stress σ_c, and the cross-sectional area of the circular strip, i.e., $\sigma_c * A_{strip(c)}$ and the tension on the end of the ellipsoidal strip is the product of ellipsoidal uniaxial stress σ_e, and the cross-sectional area of the ellipsoidal strip, i.e., $\sigma_e * A_{strip(e)}$. The force balance for the free body diagram in Fig. 5.6 is defined by the equation:

$$P_o * A_{fluid(e)} = 2\sigma_c * A_{strip(c)} + 2\sigma_e * A_{strip(e)} \qquad\qquad 5.8$$
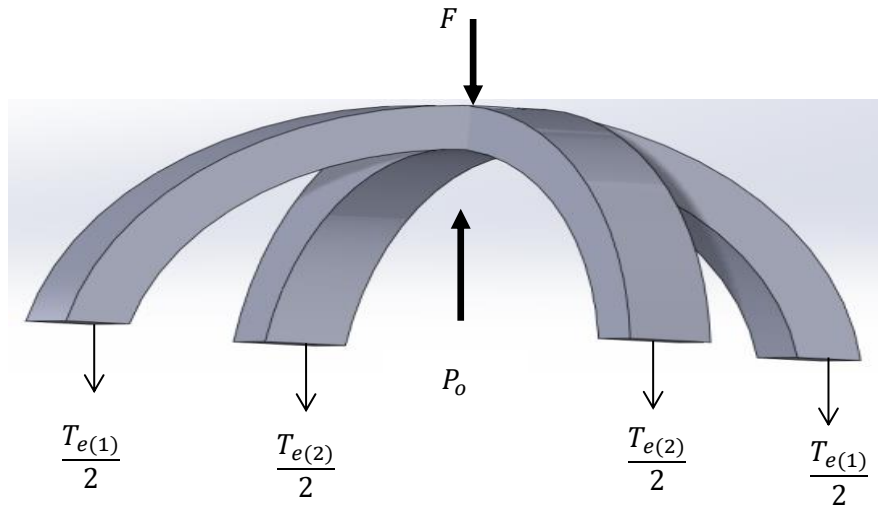
Fig. 5.7 Analysis of tension on the strips, vessel pressure and external deformation force for side view or side view of the oblate spheroid model with a side-to-side cut of two elliptical strips.

Considering the force diagram in Fig. 5.7, the upward forces are balanced by the downward forces. The upward force due to the pressure is equal to P_o times the cross-setional area of the fluid ($P_o. \pi r_c{}^2$). On the other hand, the tensile force T_e on the wall of the strips resisting the force due the pressure is given as the product of the ellipsiodal uniaxial stress and the cross-sectional area of the strip. i.e., $4\sigma_e * A_{strip(e),,}$ for the four strips. The downward force holding the

upward pressure is the sum of the the forces in the strips and the external force, F, applied to the model.

$$\frac{T_{e(1)}}{2} = \sigma_e * A_{strip(e)}; \ \frac{T_{e(2)}}{2} = \sigma_e * A_{strip(e)} \qquad 5.9$$

$$T_e = T_{e(1)} + T_{e(2)} = 4\sigma_e * A_{strip(e)}$$

$$F = P_o * A_{fluid(c)} - T_e$$

A particular fluid volume of 60 ml and undeformed pressure of 10.25 cm-H_2O were used to generate the model results in Fig. 5.8. The pressure and external force are increasing as the bladder is deformed from its original sphere shape. In addition, the length of the circular strip and ellipsoidal strips also increase as β increases. For $\beta = 0.75$, the pressure increased from 10.25 cm-H_2O to 16.86 cm-H_2O (64.49%). The wall stress in the top plane (circular strip) increased from 387.34 to 1077.40 cm-H_2O (178.53%) and increased to 547.09 cm-H_2O (41.24%) for the ellipsoidal strip. The external deformation force at the given β was 2.03 N.
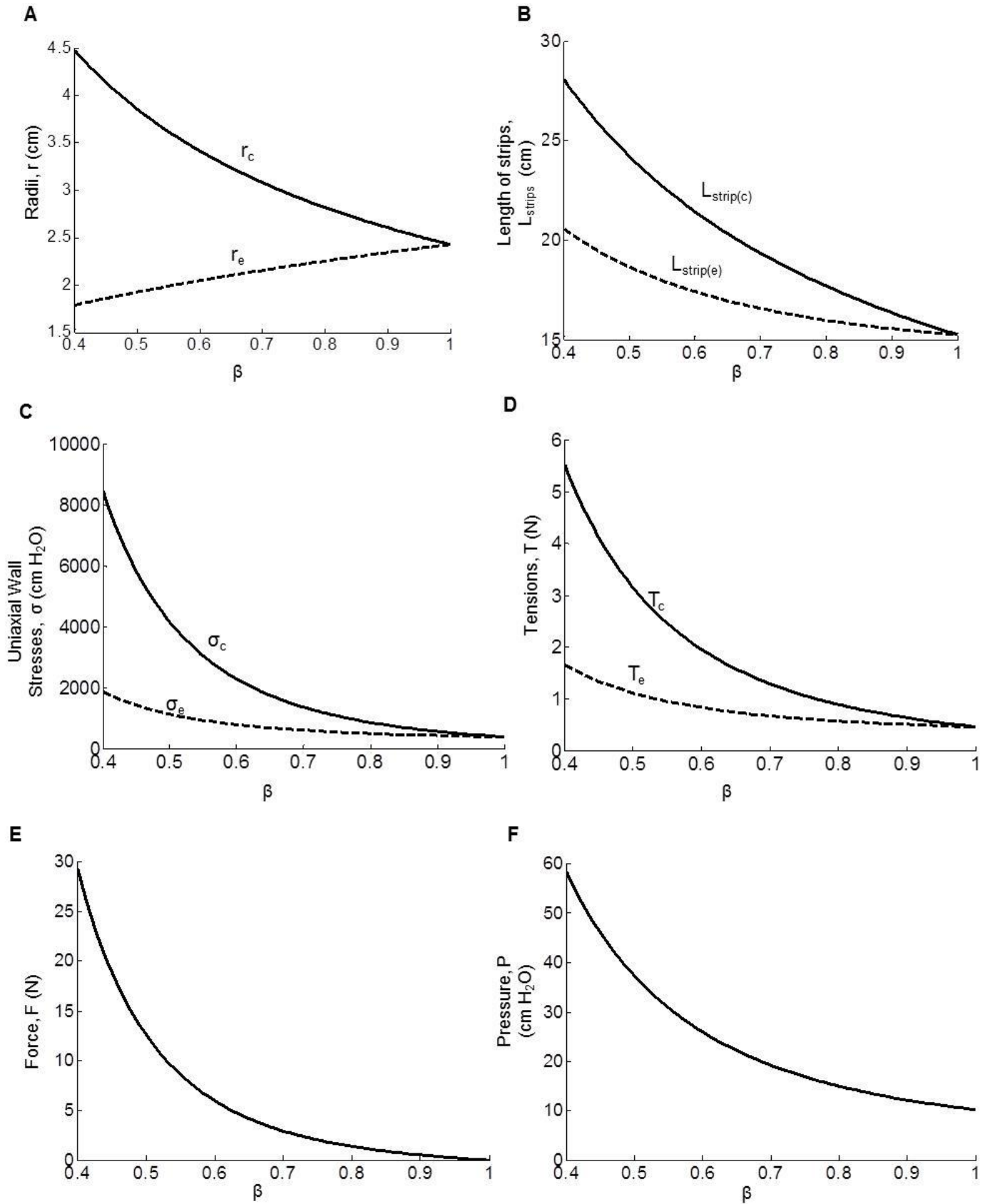
Fig. 5.8 Radius-β (**A**), Strip length-β (**B**), uniaxial wall stress-β (**C**) wall tension-β (**D**), pressure-β (**E**), and external force=β (**F**) curves predicted by the DSM model at a constant volume of V = 60 ml, and undeformed pressure P = 10.25 cm-H$_2$O, for deforming ratios ranging from 0.4 to 1 (40 – 100%), using the LCC stress-strain relationship from Fig. 3.1.

Oblate spheroid can be formed under the limits of 0<β<1. The reason why the model results only show a lower β range of 0.4 is because of the limitation of the approximation used to calculate the length of the ellipsoidal strip in equation 5.6 (Villarino, 2005). The exact formula to calculate the length of the ellipsoidal strip requires an infinite series of calculations. The β range 0.04 to 1.0 is sufficient to show the effects of deformation in Fig. 5.8.

In this model the change in the vessel pressure and wall tension were investigated when the shape is changed from sphere to an oblate spheroid using an external deformation force. The model results predict the change in stress and pressure when the bladder changes its shape acutely due to an intra-abdominal force.

Chapter Six: Conclusion

6.1. Measurement of bladder wall stress could be a valuable clinical tool

Clinical urodynamic studies currently used to diagnose overactive bladder (OAB) by measuring pressure during bladder filling. Our modeling results suggest that measurement of bladder wall stress during filling might provide valuable information for the study and diagnosis of OAB. As shown in Fig. 6.1, the model predicts that the relative change in wall stress is greater than the change in pressure during filling. Because pressure changes little during filling, we will anticipate that tension-based compliance measurements would be much more reflective of the actual tension sensor output (urgency) than standard Δvolume/Δpressure calculations. Therefore, bladder wall stress changes during filling may be a better indicator of bladder function and may correlate more closely with changes in sensation than filling pressure.
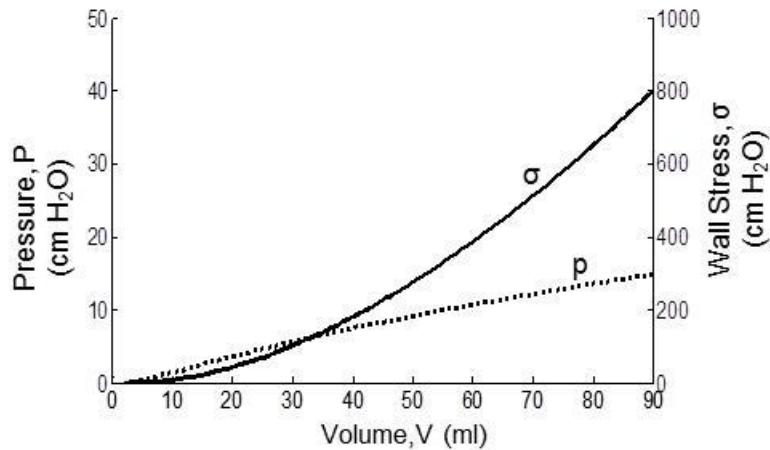
Fig. 6.1 Panel **A** from Fig. 3.2 showing modeling results for the pressure-volume and stress-volume curves for DSM with lower regulated bladder compliance.

6.2. Regulated bladder compliance could lead to urgency

The shaded area in Fig. 6.2 shows the range of wall stresses permitted by regulated detrusor compliance. A defect in regulated compliance could contribute to changes in wall stress for a given volume that could lead to urgency. Measurement of changes in regulated compliance could correlate to changes in the urgency.
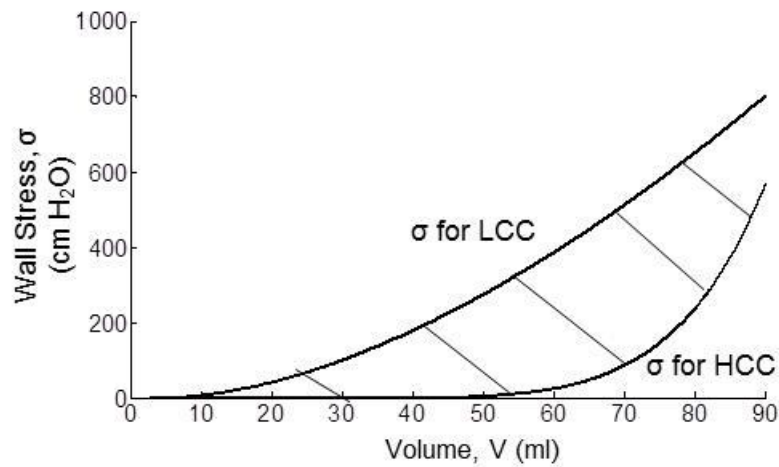
Fig. 6.2 Data from Fig. 3.3**B** showing model predictions for stress-volume curves for lower compliance (LCC) and higher compliance (HCC) stress-strain curves. The shaded area shows the range of wall stresses permitted by regulated detrusor compliance.

6.3. Bladder shape may be important to urgency

The model developed in chapter 4 demonstrates that constraining a bladder during filling can increase wall strain for a given volume (Fig. 6.3), and therefore increase wall tension and output from tension-sensitive nerves, potentially contributing to urgency. Acute or chronic changes in bladder shape due to changes in compliance or intra-abdominal forces could contribute to changes in wall stress for a given volume that could lead to urgency. Bladder shape can be measured using ultrasound and the images could be used to determine if bladder shape correlates with OAB.
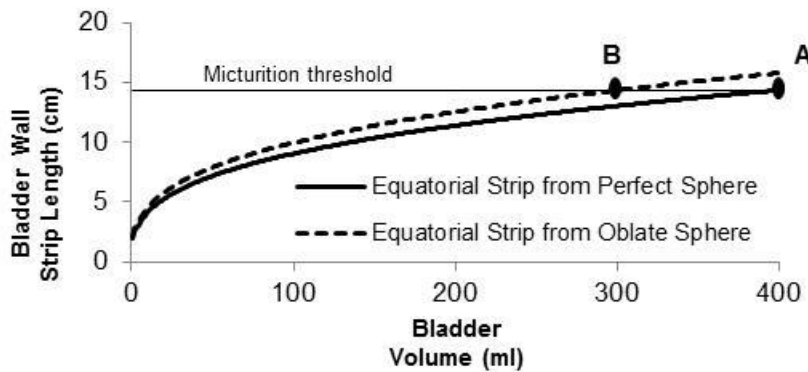
Fig. 6.3 Model results from Fig. 4.3 showing that bladder wall strip length during filling from 0 to 400 ml. A spherical bladder is assumed to reach its micturition threshold at 400 ml with an equatorial wall strip length equal to ½ the circumference, or 14.36 cm (point **A**). If the same bladder is constrained by 25% in one radial direction to form an oblate sphere, it reaches the same threshold strip length (14.36 cm) at only 300 ml (point B).

6.4. Bladder deformation may be important to urgency

Deformation of a spherical bladder into an oblate spheroid at a constant or increasing volume leads to an increase in the wall stress (Fig. 6.4) in the model developed in chapter 5. This increase in tension would be expected to increase sensation from tension-sensitive nerves and potentially increase or cause urgency.
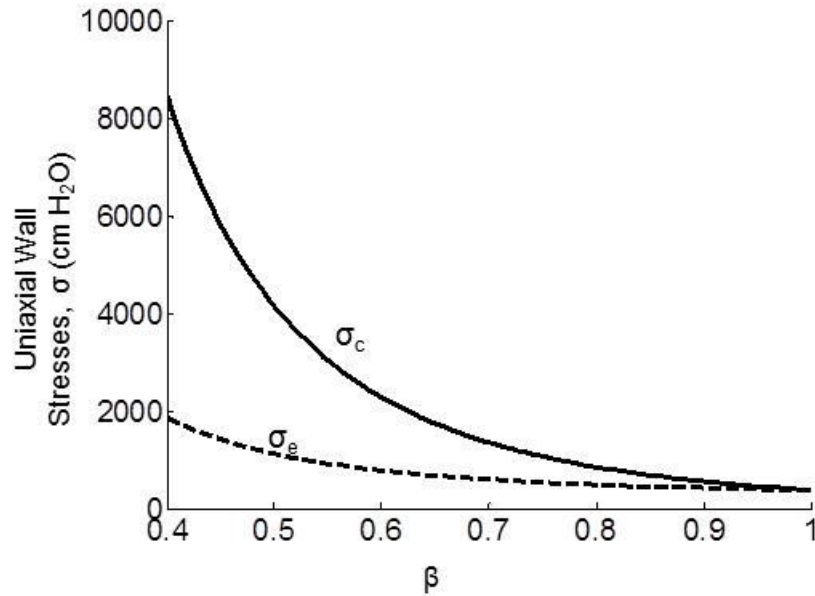
Fig. 6.4 Model results from Fig. 5.8**C** showing an increase in wall stress as a spherical bladder with β=1 is deformed by an external force into an oblate spheroid with the same volume and β<1.

Chapter Seven: Discussion and future work

7.1. Discussion

This thesis focused on modeling acute changes in bladder wall tension, shape and compliance during filling. A balloon experiment and Laplace's law were used to demonstrate that wall tension can vary significantly with geometry in a vessel with uniform pressure. The results show that the larger vessel radius had a bigger stress when it is compared to the smaller radius. Damaser et al., (Margot S Damaser & Lehman, 1993; Margot S. Damaser & Lehman, 1995). developed a model to compare filling pressure of spherical, oblate spheroid and prolate spheroid bladders at several levels of eccentricity and the model predicted that oblate bladders were more compliant than spherical or prolate bladders. The model developed in this thesis examined a shape change from a spherical bladder to an oblate spheroidal bladder by an external deformation force. Both of these studies conclude that bladder shape does matter.

Consider two rubber balloons with homogeneous material properties, one manufactured to be spherical and the other manufactured to be cylindrical. If the spherical balloon is filled with water to a particular volume of water, wall tension will increase, and if unconstrained, the balloon will maintain a spherical shape. However, if this spherical balloon is constrained to fill in a cylindrical shape, wall tension for a given volume will be elevated. Considerable effort would be required to force an isovolumetric spherical water balloon into a cylindrical shape. Likewise, if the originally cylindrical balloon is filled with water, wall tension will increase, and if unconstrained, the balloon will maintain a cylindrical shape. However, if this cylindrical balloon is constrained to fill as a sphere, wall tension for a given volume will be elevated. Thus, the initial relaxed shape of the balloon material affects the wall tension during either constrained or unconstrained filling. Thus, for a bladder with a relaxed shape that is not spherical, filling in the shape of a sphere would increase wall stress. Therefore, studying bladder shape change during filling may be more important than the shape itself.

Published experimental data (Speich, Dosier et al. 2007) were used to determine ranges for regulated detrusor compliance and to expand a finite deformation model of bladder filling to illustrate the potential effects of acute regulation of compliance on filling pressure and wall stress

(Janz et al., 1980; Saito & Oki, 1982; Watanabe et al., 1981). Watanabe et al. concluded from their experimental and modeling results that the relatively flat pressure-volume curve observed during clinical cystomety could be produced by the elasticity of the bladder itself, without the need for neural feedback (Watanabe, Akiyama et al. 1981). In this thesis, a finite deformation continuum model was compared with a constant pressure model. The results from the continuum model show that a defect in regulated compliance could contribute to changes in wall stress for a given volume that could lead to urgency.

A geometric model was used to demonstrate that changes in bladder shape due to changes in compliance or intra-abdominal forces could contribute to changes in wall tension for a given volume that could lead to urgency. A three-ring spheroidal bladder model was developed to examine pressure and wall tension changes during deformation. The results show that for a particular fluid volume and initial pressure, the pressure and external force increase as the bladder is deformed from its original spherical shape into an oblate spheroid. In addition, the circumference (length) of circular and ellipsoidal strips rise as the bladder is deformed. The minor radius of ellipsoidal strip is β fraction of the major radius of the ellipsoidal strip, the rate of increase of the major radius is greater than the rate of decrease of the minor radius; therefore the circumference increases. Thus, both the stresses on circular and ellipsoidal strips are increase with bladder deformation, and since the bladder does not likely have uniform properties everywhere within the wall, it is probable that any tension sensors positioned throughout the wall of the bladder sense different stresses, which could affect bladder fullness information transmitted to the brain. Thus, deformation leads to increased wall stresses which would be expected to increase bladder sensation and potentially cause urgency.

7.2. Future work

The model developed in this thesis was based on experimental uniaxial tension data. In a uniaxial extension test for a sample clamped at the ends, the other dimensions of the strip are not constrained. However, this is not the case in an intact bladder; therefore, a biaxial extension test could be employed to better approximate true behavior in the model. Furthermore, during filling the bladder experiences three dimensional shape changes, i.e., the length, the thickness and the

width of a strip change. Therefore, measuring the stress-strain relationship in intact bladders may provide better data for developing models to simulate the behavior of the bladder during filling.

The modeling results in chapter 3 showed that there was a small change in pressure but wall stress was significantly increasing with volume during filing, and wall stress may give better information about the change in bladder compliance during filling. As a result, measuring wall stress during clinical urodynamics may be a good research topic to work on the future. This will require a development of a method of measuring wall tension directly, like a strain gauge, or approximating wall tension from pressure data obtained from the usual urodynamics procedure and the addition of bladder geometry information, possibly from ultrasound images.

Normal bladders vary in shape, and bladder compliance has been shown to depend on shape (Zhang, Wu, Xi, Wang, & Jiang, 2012). Ultrasonic estimation of bladder volume can be affected by the variations in bladder shape (Bih, Ho, Tsai, Lai, & Chow, 1998). Bladder shape can be measured using ultrasound and the images could be used to determine if bladder shape correlates with OAB. The effect of shape change in bladder compliance was shown in chapter 5 for a case when a bladder changes its original sphere shape to an oblate one due to an external deformation force. This effect may be observed in other bladder shapes mentioned in Fig. 1.3 and therefore, three-ring spheroidal model can be extended for these non-spheroidal bladder shapes.

The experimental stress-strain data used to develop the models in this thesis were taken from rabbit bladder strips (Speich et al., 2007). In addition, an assumption can be made that the experimental stress-stain curve from rabbit bladder in Fig. 3.1 has the same properties as human bladder. Then these data can be used to predict possible changes in pressure and stress in human bladder as performed for rabbit bladder in chapter 3. However, measurement of stress-strain curves for human bladder tissue and quantifying any regulated bladder compliance in humans would improve the quality of model and simulations of how regulated compliance and shape change could affect wall stresses during human bladder filling.

References

Abrams, P., Cardozo, L., Fall, M., Gri, D., Rosier, P., Ulmsten, U., … Wein, A. (2002). The Standardisation of Terminology of Lower Urinary Tract Function : Report from the Standardisation Sub-committee of the International Continence Society, *178*, 167–178.

Abrams, P., & Wein, A. J. (2000). Introduction: Overactive bladder and its treatment. *Urology*, *55*, 1–2.

Almasri, A. M., Ratz, P. H., Bhatia, H., Klausner, A. P., & Speich, J. E. (2010). Rhythmic contraction generates adjustable passive stiffness in rabbit detrusor. *J Appl Physiol*, *108*(3), 544–553.

Almasri, A. M., Ratz, P. H., & Speich, J. E. (2010). Length adaptation of the passive-to-active tension ratio in rabbit detrusor. *Ann Biomed Eng*, *38*(8), 2594–2605.

Andersson, K. E., & Arner, A. (2004). Urinary bladder contraction and relaxation: physiology and pathophysiology. *Physiol Rev*, *84*(3), 935–986.

Bechir, H., Chevalier, L., Chaouche, M., & Boufala, K. (2006). Hyperelastic constitutive model for rubber-like materials based on the first Seth strain measures invariant. *European Journal of Mechanics - A/Solids*, *25*(1), 110–124.

Bih, L.-I., Ho, C.-C., Tsai, S.-J., Lai, Y.-C., & Chow, W. (1998). Bladder shape impact on the accuracy of ultrasonic estimation of bladder volume. *Archives of Physical Medicine and Rehabilitation*, *79*(12), 1553–1556.

Chancellor, M. B., Oefelein, M. G., & Vasavada, S. (2010). Obesity is associated with a more severe overactive bladder disease state that is effectively treated with once-daily administration of trospium chloride extended release. *Neurourol Urodyn*, *29*(4), 551–554.

Chancellor, M. B., Rivas, D. A., & Bourgeois, I. M. (1996). Laplace's law and the risks and prevention of bladder rupture after enterocystoplasty and bladder autoaugmentation. *Neurourol Urodyn*, *15*(3), 223–233.

Damaser, M. S., & Lehman, S. L. (1993). Does it Matter , the Shape of tha bladder? *Neuroulogy and Urodynamics*, *14*, 277–280.

Damaser, M. S., & Lehman, S. L. (1993). Does it matter, the shape of the bladder? *Neurourol Urodyn*, *12*(3), 277–280.

Damaser, M. S., & Lehman, S. L. (1995). The Effect of Urinary Bladder Shape on its Mechanics During Filling. *J Biomech*, *28*(6), 725–732.

Fata, B., Carruthers, C. A., Gibson, G., Watkins, S. C., Gottlieb, D., Mayer, J. E., & Sacks, M. S. (n.d.). Regional structural and biomechanical alterations of the ovine main pulmonary artery during postnatal growth. *J Biomech Eng*, *135*(2), 21022.

Frenkl, T. L., Railkar, R., Palcza, J., Scott, B. B., Alon, A., Green, S., & Schaefer, W. (2011). Variability of urodynamic parameters in patients with overactive bladder. *Neurourol Urodyn*, *30*(8), 1565–1569.

Fujii, T., Takagi, H., Arimoto, M., Ootani, H., & Ueeda, T. (2000). Bundle formation of smooth muscle desmin intermediate filaments by calponin and its binding site on the desmin molecule. *J Biochem (Tokyo)*, *127*(3), 457–465.

Fung, Y. C. (1993). *Biomechanics: Mechanical Properties of Living Tissues* (2nd ed.). New York: Springer-Verlag.

Hashim, H., & Abrams, P. (2007). Overactive bladder: an update. *Current Opinion in Urology*, *17*(4), 231–6.

Hibbeler, R. C. (2011). *Mechanics of materials* (8th ed., p. xv, 862 p.). Boston: Prentice Hall.

Hubeaux, K., Deffieux, X., Desseaux, K., Verollet, D., Damphousse, M., & Amarenco, G. (2012). Stand up urgency: is this symptom related to a urethral mechanism? *Progrès En Urologie : Journal de l'Association Française D'urologie et de La Société Française D'urologie*, *22*(8), 475–81.

Janz, R. F., Kubert, B. R., Pate, E. F., & Moriarty, T. F. (1980). Effect of Shape on Pressure-Volume Relationships of Ellipsoidal Shells. *American Journal of Physiology*, *238*(6), H917–H926.

Kanai, A., & Andersson, K. E. (2013). Bladder afferent signaling: recent findings. *J Urol*, *183*(4), 1288–1295.

Kim, J. H., Lee, J. H., Jung, A. Y., & Lee, J. W. (2011). The prevalence and therapeutic effect of constipation in pediatric overactive bladder. *Int Neurourol J*, *15*(4), 206–210.

Korkmaz, I., & Rogg, B. (2007). A simple fluid-mechanical model for the prediction of the stress-strain relation of the male urinary bladder. *Journal of Biomechanics*, *40*(3), 663–8.

Mahfouz, W., Al Afraa, T., Campeau, L., & Corcos, J. (2012). Normal urodynamic parameters in women: part II--invasive urodynamics. *International Urogynecology Journal*, *23*(3), 269–77.

Matsumoto, S., Chichester, P., Bratslavsky, G., Kogan, B. A., & Levin, R. M. (2002). The functional and structural response to distention of the rabbit whole bladder in vitro. *The Journal of Urology*, *168*(6), 2677–81.

Miftahof, R. N., & Nam, H. G. (2013). *Biomechanics of the Human Urinary Bladder* (p. 188). Springer-Verlag.

Muhr, A. H. (2005). Modeling the Stress-Strain Behavior of Rubber. *Rubber Chemistry and Technology*, *78*(3), 391–425.

Ockrim, J., Laniado, M. E., Khoubehi, B., Renzetti, R., Finazzi Agro, E., Carter, S. S., & Tubaro, A. (2005). Variability of detrusor overactivity on repeated filling cystometry in men with urge symptoms: comparison with spinal cord injury patients. *BJU Int*, *95*(4), 587–590.

Ratz, P. H., & Speich, J. E. (2010). Evidence that actomyosin cross bridges contribute to "passive" tension in detrusor smooth muscle. *Am J Physiol Renal Physiol*, *298*(6), F1424–35.

Rose, D. K. (1927). Determination of Bladder Pressure with the Cystometer: A New Principle in Diagnosis. *Journal of the American Medical Association*, *88*(3), 151–157.

Saito, T., & Oki, F. (1982). The strain-energy density function of the urinary bladder. *The Tohoku Journal of Experimental Medicine*, *137*(4), 401–8.

Schwartz, S. M., & Mecham, R. P. (1995). *The Vascular Smooth Muscle Cell : Molecular and Biological Responses to the Extracellular Matrix*. San Diego: Academic Press.

Speich, J. E., Almasri, A. M., Bhatia, H., Klausner, A. P., & Ratz, P. H. (2009). Adaptation of the length-active tension relationship in rabbit detrusor. *Am J Physiol Renal Physiol*, *297*(4), F1119–28.

Speich, J. E., Borgsmiller, L., Call, C., Mohr, R., & Ratz, P. H. (2005). ROK-induced cross-link formation stiffens passive muscle: reversible strain-induced stress softening in rabbit detrusor. *Am J Physiol Cell Physiol*, *289*(1), C12–21.

Speich, J. E., Dosier, C., Borgsmiller, L., Quintero, K., Koo, H. P., & Ratz, P. H. (2007). Adjustable passive length-tension curve in rabbit detrusor smooth muscle. *J Appl Physiol*, *102*(5), 1746–1755.

Speich, J. E., Quintero, K., Dosier, C., Borgsmiller, L., Koo, H. P., & Ratz, P. H. (2006). A mechanical model for adjustable passive stiffness in rabbit detrusor. *J Appl Physiol*, *101*(4), 1189–1198.

Speich, J. E., Southern, J. B., Henderson, S., Wilson, C. W., Klausner, A. P., & Ratz, P. H. (2012). Adjustable passive stiffness in mouse bladder: regulated by Rho kinase and elevated following partial bladder outlet obstruction. *Am J Physiol Renal Physiol*, *302*(8), F967–76.

Valanis, K. C. (1967). The Strain-Energy Function of a Hyperelastic Material in Terms of the Extension Ratios. *Journal of Applied Physics*, *38*(7), 2997.

Van Brummen, H. J., Bruinse, H. W., van de Pol, G., Heintz, A. P., & van der Vaart, C. H. (2006). Bothersome lower urinary tract symptoms 1 year after first delivery: prevalence and the effect of childbirth. *BJU Int*, *98*(1), 89–95.

Villarino, M. B. (2005). Ramanujan's Perimeter of an Ellipse, 12. Classical Analysis and ODEs; General Mathematics.

Watanabe, H., Akiyama, K., Saito, T., & Oki, F. (1981). A finite deformation theory of intravesical pressure and mural stress of the urinary bladder. *The Tohoku Journal of Experimental Medicine*, *135*(3), 301–7.

Zhang, Y., Wu, S., Xi, Z., Wang, X., & Jiang, X. (2012). Measuring diagnostic accuracy of imaging parameters in pelvic lipomatosis. *European Journal of Radiology*, *81*(11), 3107–14.

Vita

Firdaweke Goraw Habteyes was born in Addis Ababa, Ethiopia. After completing his work at Medhanialem High School, Addis Ababa, Ethiopia, in 2005, he entered Bahir Dar University in Bahir Dar, Ethiopia. He received the degree of Bachelor of Science from Bahir Dar University in July 2009 with Industrial Engineering major. During the following years, he was employed as a Graduate Assistant and Assistant Lecturer at Bahir Dar University. In August, 2012, he entered the Graduate School at Virginia Commonwealth University, Richmond, Virginia.

Permanent Address: 4814 Willow Stead Drive

Olney, Maryland 20832

firdefigo@gmail.com

This thesis was typed by the author.